IEEE Access
Multidisciplinary | Rapid Review | Open Access Journal

Received 22 March 2023, accepted 7 April 2023, date of publication 12 April 2023, date of current version 17 April 2023.

Digital Object Identifier 10.1109/ACCESS.2023.3266279

RESEARCH ARTICLE

Torque Analytical Calculation of Formed Winding Permanent Magnet Motor

KE ZHANG, YANPING LIANG, XU BIAN, AND PEIPEI YANG
College of Electronic Engineering, Harbin University of Science and Technology, Harbin 150080, China

Corresponding author: Yanping Liang (liangyanping2010@126.com)

This work was supported in part by the National Natural Science Foundation of China under Grant 51977053.

ABSTRACT The development of electrification has put forward higher requirements for the efficiency and power density of permanent magnet motors. The combination of formed flat wire windings and open slots with rectangular cross-sections has been applied in permanent magnet motors, which makes the motor torque fluctuate significantly, and the vibration and noise caused by it seriously influence the stability of operation. Therefore, it is essential to study the torque characteristics for permanent magnet motors with formed windings. The open slot brings rich tooth harmonics to the air-gap magnetomotive force. In this study, an analytical model of the motor magnetic field was established based on magnetic potential and relative permeance theory. According to the Lorentz force law, an analytical model of the instantaneous torque of the permanent magnet motor with a formed winding is derived. The model points out that under the modulation of the relative permeance function, the constant torque and torque fluctuation are generated after the interaction of the stator magnetomotive force and rotor magnetic potential that meet the corresponding harmonic order relationship, and the order of the torque fluctuation is a multiple of 6. According to the analytical model, different torque components of the permanent magnet motor with formed windings are calculated and verified by the finite element method.

INDEX TERMS Formed winding, Lorentz force law, magnetic field calculation, permanent magnet motor, torque characteristic.

I. INTRODUCTION

The permanent magnet (PM) motor has a simple structure, high efficiency, and strong field weakening ability. It is widely used in the fields of new energy vehicles, aerospace, and industrial drive systems [1], [2]. With the development of high speed and the improvement of power level, the efficiency and power density of PM motors are required to be higher. The characteristics of high filling factor and short end size of flat wire winding can further improve the efficiency and power density [3], [4], and become the choice of the high-performance motor system. Therefore, PM motors started to be equipped with formed windings wound by flat conductors and embedded in open slots with rectangular cross-sections [5]. However, the application of open slots makes the motor torque ripple severe, and the vibration and noise caused by it seriously affect the stability of the motor operation.

The formed winding is simple in structure and adopts a preformed structure, which avoids the twisting and welding steps compared to hairpin winding. However, due to its radial insertion mode, the PM motor with formed windings can only adopt the slot structure with open slots. Reference [6] takes an open-slot-type interior permanent magnet (IPM) motor to compare the torque ripple of four slot structures, including an open slot, a semi-open slot, an open slot with the wedge, and a semi-closed slot, among which the open slot is the most significant. Reference [7] calculated the torque characteristics of the ultra-high-speed axial flux permanent magnet (AFPM) motor under slotting and slotless conditions by using the analytical method (AM), and the analysis showed that the slotted motor improved the output torque as while as the torque fluctuation. Therefore, for the PM motor with formed windings, it is essential to establish an analytical model

The associate editor coordinating the review of this manuscript and approving it for publication was Jinquan Xu.

This work is licensed under a Creative Commons Attribution-NonCommercial-NoDerivatives 4.0 License.
For more information, see https://creativecommons.org/licenses/by-nc-nd/4.0/

between the motor parameters and torque, and accurately calculate the motor torque characteristics.

Accurate calculation of the magnetic field is the basis for obtaining the torque characteristics. For PM motors, the main methods include the equivalent magnetic network (EMN) method, subdomain method, and magnetic potential-permeance analytical model. The EMN divides the nodes according to the motor magnetic circuit and the influence of iron core saturation can be considered through iterative permeability [8]. The sub-domain method requires that the magnetic field solution region has a radial boundary, which is more used in surface-mounted rotor structures [9] and permanent magnet vernier motors [10]. However, the rotor structure of IPM motors is complex and the radial boundary conditions are difficult to determine. When solving the magnetic field, the magnetic potential and permeance model obtain the magnetic potential with the help of winding function theory and equivalent magnetic circuit (EMC) method, and then use the permeance model to solve the magnetic field [11], [12], [13], but it usually ignores the saturation of the rotor bridge area.

The torque calculation of PM motors has been widely studied. The FEM can accurately simulate the actual structure of the motor and effectively solve the problem of ferromagnetic material saturation. Reference [14] took a switched reluctance motor as an example, the influence of current harmonics on torque characteristics is studied and adopted the frozen permeability method considers magnetic saturation under different current excitation. However, its accuracy and calculation time are affected by the quality of the mesh. The main AMs include the Maxwell stress tensor method [15], [16] and the Lorentz force law [17], [18]. When calculating torque, the former needs to solve the tangential component of the magnetic field, which is usually solved by FEM [19] and the subdomain method [20], this is not only difficult to establish the analytical relationship between electromagnetic parameters and torque; but also not applicable to interior rotor structure. The Lorentz force law establishes an analytical model between electromagnetic parameters and torque by considering the interplay between the stator magnetomotive force (MMF) and rotor magnetic potential (RMP); and investigates the effect of different parameters on torque. Reference [21] derived the instantaneous torque model of the variable flux reluctance motor based on Lorentz force law and analyzed the synchronous torque, reluctance torque, and cogging torque, but the PM torque cannot be calculated due to the different motor structures. Reference [22] derived the torque model of a five-phase interior permanent magnet synchronous motor (IPMSM) by using Lorentz force law and reduced the torque ripple by moving the asymmetric pole, but the influence of stator slotting is ignored.

In this paper, based on the magnetic potential and relative permeance theory, the motor magnetic field is solved by using the winding function and EMC method. According to the magnetic field modulation theory, the change of harmonic component of stator and rotor magnetic potential is obtained under the action of air gap relative permeance function. Then the formed winding PM motor transient torque calculation model is established according to the Lorentz force law. Based on the analytical model, the effect of the interaction of stator and rotor magnetic potential harmonics and relative permeance harmonics on the torque characteristics is studied. Finally, different torque components of PM torque, reluctance torque, and electromagnetic torque are obtained based on the torque analysis model.

II. MOTOR TORUE AND MMF

When the stator tooth slot effect is ignored in the PM motor with formed windings, assuming that the stator inner radius is smooth and that armature winding can be equivalent to an infinite thin current sheet at the inner diameter of the stator, the following relationship exists between the MMF and the electrical load excited by the armature current:

$$r_g K_s(\theta, t) = \frac{\mathrm{d}F_s(\theta, t)}{\mathrm{d}\theta} \tag{1}$$

where: r_g is the radius in the middle of the air gap, θ is the mechanical angle in the stator coordinate system.

For an IPM motor with a smooth rotor surface, the flux density can be calculated as:

$$B(\theta, t) = (F_s(\theta, t) - F_r(\theta, t))\frac{\mu_0}{g} \tag{2}$$

where: $F_r(\theta, t)$ is the RMP, μ_0 is the air permeability; g is the air gap length.

According to the Lorentz force law, the Lorentz force density is integrated along the radius of the middle air gap to obtain the instantaneous torque expression:

$$T_e = -r_g l_{ef} \int_0^{2\pi} K_s(\theta, t) B(\theta, t) r_g \mathrm{d}\theta \tag{3}$$

where: l_{ef} is the axial length.

Substituting (1) and (2) into (3) to obtain:

$$\begin{aligned} T_e &= -r_g l_{ef} \int_0^{2\pi} B(\theta, t)\mathrm{d}F_s(\theta, t) \\ &= -r_g l_{ef} \frac{\mu_0}{g} \int_0^{2\pi} (F_s(\theta, t) - F_r(\theta, t))\mathrm{d}F_s(\theta, t) \end{aligned} \tag{4}$$

Considering the stator slotting, the air gap relative permeance function is related to the air gap length g and the corresponding flux path length $g_s(\theta)$ at the stator slot, then the air gap relative permeability function is as follows:

$$\Lambda_s(\theta) = \frac{g}{g_s(\theta) + g} \tag{5}$$

Under one stator pitch, the length of the magnetic flux path corresponding to the stator slot is [23]:

$$g_s(\theta) = \begin{cases} \dfrac{\pi R_{si} \sin\frac{\theta}{2} \sin(\frac{\alpha_b}{2} - \frac{\theta}{2})}{2 \sin\frac{\alpha_b}{4} \cos(\frac{\theta}{2} - \frac{\alpha_b}{4})}; & \theta \in [0, \alpha_b] \\ 0; & \theta \in \left[\alpha_b, \alpha_{t_1}\right] \end{cases} \tag{6}$$

where: α_b is the width angle of stator slot, $\alpha_b = b/R_{si}$. b and R_{si} are stator slot width and stator inner radius respectively. α_{t1} is the stator pitch angle, $\alpha_{t_1} = t_1/R_{si}$. t_1 is stator pitch.

According to (5), taking the motor studied in this paper as an example, the air gap relative permeance function after slotting is considered as shown in Fig. 1.

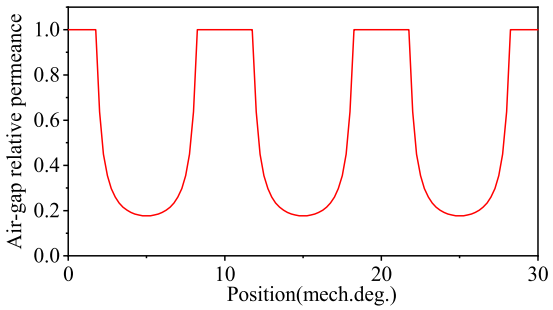

FIGURE 1. Air-gap relative permeance waveform.

$\Lambda_s(\theta)$ can be expanded by the Fourier series as follows:

$$\Lambda_s(\theta) = \Lambda_{s0} + \sum_{k=1}^{\infty} \Lambda_{sk} \cos(kZ\theta) \tag{7}$$

where: k is the harmonic number, Λ_{s0} is the constant current component, Λ_{sk} is k th-order harmonic component coefficient, Z is the number of stator slots.

Then flux density after stator slotting can be expressed as:

$$B(\theta, t) = (F_s(\theta, t) - F_r(\theta, t))\frac{\mu_0}{g}\Lambda_s(\theta) \tag{8}$$

According to (8), after the stator slotting, the air gap magnetic density and instantaneous torque are related to the stator MMF, RMP, and air-gap specific permeability function.

III. AIR GAP MAGNETIC POTENTIAL

In this paper, a 36-slot and 8-pole PM motor with formed windings is taken as an example to calculate the magnet potential and analyze the torque characteristics. The structure of the formed winding PM motor is shown in Fig.2. The stator side uses a rectangular open slot with formed winding. The rotor side adopts an interior rotor structure and the motor parameters are shown in Table 1.

A. WINDING FUNCTION THEORY AND STATOR MMF

For the pole slot coordination of 36 slots and 8 poles, take the A-phase winding as an example, the winding function distribution is shown in Fig. 3, where N_1 is the number of coil turns.

The armature MMF is obtained by multiplying the winding function and the applied excitation. As shown in Fig. 2, at the space mechanical angle θ from the axis of phase A, the winding functions of three-phase windings A, B, and C are

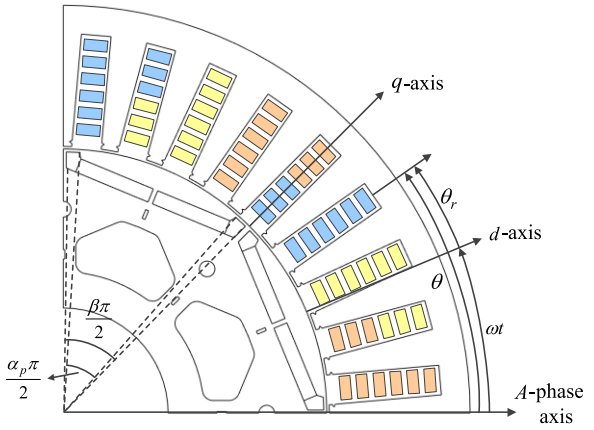

FIGURE 2. Structure of interior PM motor with formed winding.

TABLE 1. Parameters of formed winding PM motor.

Quantity	Unit	Value
Rated power	kW	15
Rated speed	r/min	2550
Stator outer radius	mm	130
Stator inner radius	mm	85
Air gap length	mm	0.8
Axial length	mm	155
Current amplitude	A	64.35
Winding pitch	-	4
Number of conductors per slot	-	6
Phase number	-	3
PM material	-	N40SH
Core material	-	50W600

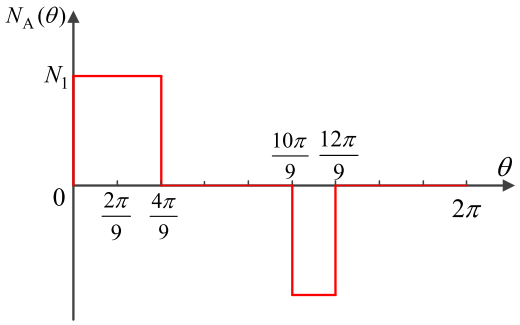

FIGURE 3. A-phase winding function distribution.

as follows:

$$\begin{cases} W_a(\theta) = \sum_v \dfrac{2Nk_{wv}}{vp\pi} \cos v(p\theta) \\ W_b(\theta) = \sum_v \dfrac{2Nk_{wv}}{vp\pi} \cos v(p\theta - \dfrac{2}{3}\pi) \\ W_c(\theta) = \sum_v \dfrac{2Nk_{wv}}{vp\pi} \cos v(p\theta - \dfrac{4}{3}\pi) \end{cases} \tag{9}$$

where: N is the number of turns in series of single phase of the formed winding, v represents harmonic order, k_{wv} is the winding factor, p is the number of pole pairs.

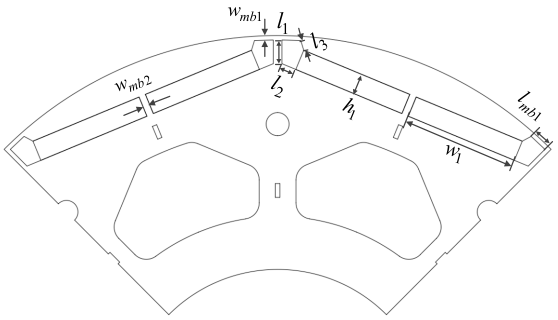

FIGURE 4. Rotor topology.

TABLE 2. Rotor geometry parameters.

Symbol	Value	Symbol	Value
h_1	4.5 mm	w_{mb2}	1.5mm
w_1	25 mm	l_1	5.14mm
w_{mb1}	0.95mm	l_2	3.26mm
l_{mb1}	4.1mm	l_3	2.19mm

The three-phase symmetrical current through the armature winding is:

$$\begin{cases} i_a(t) = \sqrt{2} I_\varphi \cos(\omega t - \varphi) \\ i_b(t) = \sqrt{2} I_\varphi \cos(\omega t - \varphi - 2\pi/3) \\ i_c(t) = \sqrt{2} I_\varphi \cos(\omega t - \varphi - 4\pi/3) \end{cases} \tag{10}$$

where: I_φ is the RMS value of stator armature current, ω is the rotor angular velocity, and φ is the current initial phase angle.

The armature MMF generated by the winding function and current are as follows:

$$\begin{aligned} F_s(\theta, t) &= W_a i_a + W_b i_b + W_c i_c \\ &= \sum_v 1.35 \frac{N k_{wv} I_\phi}{vp} \cos(vp\theta - k_v \omega t + k_v \varphi) \\ &= \sum_v F_{sv} \cos(vp\theta - k_v \omega t + k_v \varphi) \end{aligned} \tag{11}$$

where:

$$\begin{cases} k_v = 1, v = 3i + 1 \\ k_v = -1, v = 3i + 2 \\ i = 0, 1, 2, \ldots \end{cases} \tag{12}$$

B. RMP

Fig. 4 shows a two-dimensional cross-sectional view of the motor rotor, to improve the magnetic weakening ability, the PM adopts an I-shaped interior structure, and its parameters are listed in Table 2. For the IPMSM, in addition to the RMP generated by the PM, the upper part of the magnetic barrier can be seen as an equipotential region, where the magnetic voltage drop can be calculated by the RMP generated by the stator armature current. The rotor bridge area of the IPMSM is saturated, to accurately calculate the RMP, the influence of saturation needs to be considered.

TABLE 3. Combination that produces average torque.

condition	Λ_{sk}	F_{sv}	F_{rh}
$vp = hp$	$k = 0$	$v = 1$	$h = 1$
$vp = hp + kZ$	$k = 1$	$v = 10$	$h = 1$
	$k = 1$	$v = 19$	
	$k = 1$	$v = 28$	
	…	…	
$vp = \lvert hp - kZ \rvert$	$k = 1$	$v = 8$	$h = 1$
	$k = 1$	$v = 17$	
	$k = 1$	$v = 26$	
	…	…	

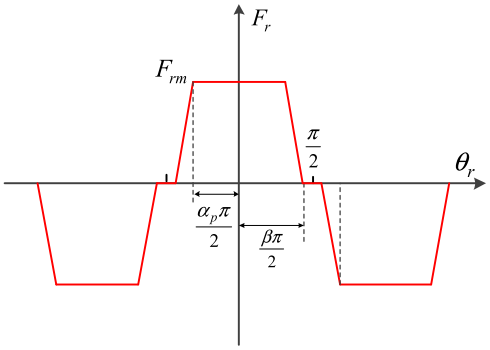

FIGURE 5. PM magnetic potential model.

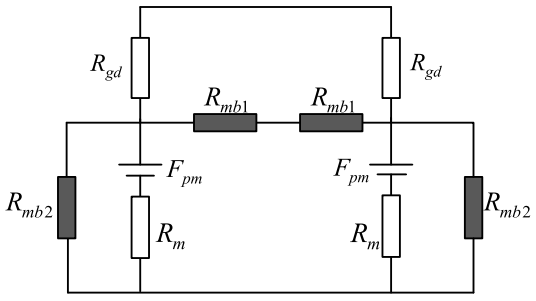

FIGURE 6. EMC model.

When only the PM acts, the simplified magnetic potential model generated by the PM is shown in Fig. 5. The rotor bridge area is heavily saturated, and the rest of the motor is not saturated, so stator reluctance and rotor reluctance can be ignored. The EMC model is given in Fig.6. In the figure: R_{gd} is the air gap reluctance at half pole pitch; F_{pm} is the equivalent magnetic potential source of the PM, R_m is corresponding PM reluctance; R_{mb1} and R_{mb2} represent the reluctance at magnetic bridge $mb1$ and $mb2$ respectively, and there is saturation overflow at the magnetic bridge $mb1$, whose saturation length is considered as $l = l_{mb1} + 2w_{mb1}$ [24]. The parameters in the EMC are calculated as follows:

$$R_m = \frac{h_1}{\mu_0 \mu_r w_1 l_{ef}} \tag{13}$$

$$F_{pm} = \frac{B_r h_1}{\mu_0 \mu_r} \tag{14}$$

$$R_{gd} = \frac{2g_e}{\alpha_p \mu_0 \pi r_g l_{ef}} \tag{15}$$

$$R_{mb1} = \frac{l}{\mu_0 \mu(B_{mb1}) w_{mb1} l_{ef}} \tag{16}$$

$$R_{mb2} = \frac{h_1}{\mu_0 \mu(B_{mb2}) w_{mb2} l_{ef}} \tag{17}$$

where: h_1 is the length of magnetization direction, w_1 is the width of PM; B_r is remanence, μ_r is the relative permeability of the PM; w_{mb1} and w_{mb2} are the widths of the magnetic bridge $mb1$ and bridge $mb2$ respectively; g_e is the equivalent air gap length after considering the stator slotting [11]; $\mu(B_{mb1})$ and $\mu(B_{mb2})$ are the relative permeability of magnetic bridge $mb1$ and bridge $mb2$ respectively.

According to Fig. 6 and (13)-(17), the RMP generated by the PM at no load can be expressed as:

$$F_{rm} = \frac{F_{pm}/R_m}{1/R_m + 1/R_{mb1} + 1/R_{mb2} + 1/R_{gd}} \tag{18}$$

The RMP can be expressed as:

$$F_r(\theta_r) = \begin{cases} F_{rm}, & 0 \le \theta_r < \dfrac{\alpha_p \pi}{2} \\ -KF_{rm}(\theta_r - \beta\pi/2), & \dfrac{\alpha_p \pi}{2} \le \theta_r < \dfrac{\beta\pi}{2} \\ 0, & \dfrac{\beta\pi}{2} \le \theta_r < \dfrac{\pi}{2} \\ 0, & \dfrac{\pi}{2} \le \theta_r < \pi - \dfrac{\beta\pi}{2} \\ KF_{rm}(\theta_r - \pi + \beta\pi/2), & \pi - \dfrac{\beta\pi}{2} \le \theta_r < \pi - \dfrac{\alpha_p \pi^2}{2} \\ -F_{rm}, & \pi - \dfrac{\alpha_p \pi}{2} \le \theta_r < \pi \end{cases} \tag{19}$$

where: $K = 1/(\beta\pi/2 - \alpha_p\pi/2)$; θ_r is the rotor mechanical angle; $\alpha_p$is the pole-arc coefficient of PM, β is the bridge arc-to-pole arc coefficient.

The RMP is expanded by the Fourier series as follows:

$$\begin{aligned} F_r(\theta, t) &= \sum_h^{\infty} \frac{8F_{rm}(\cos(h\frac{\alpha_p}{2}\pi) - \cos(h\frac{\beta}{2}\pi))}{h^2\pi^2(\beta - \alpha_p)} \cos(ph\theta_r) \\ &= \sum_h^{\infty} F_{rh} \cos(ph\theta - hwt) \end{aligned} \tag{20}$$

where: F_{rh} is the coefficient of the hth-order harmonic.

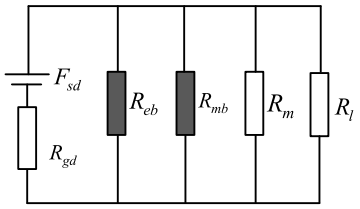

FIGURE 7. EMC model of armature field.

When only the d-axis armature current acts, the rotor bridge region is in saturation. Then the magnetic potential distribution of the d-axis rotor is the same as that of the PM rotor model, only the amplitude is different. The rotor magnetic flux is divided into four parts, passing through the PM, magnetic barrier, magnetic bridge $mb1$ and magnetic bridge $mb2$ respectively. According to the rotor magnetic flux path, the magnetic potential can be expressed as (21) and (22), shown at the bottom of the page, where:

$$\begin{cases} \Lambda_1 = \frac{\mu_0}{pg_e} r_g l_{ef} \\ \Lambda_2 = \frac{\mu_0 \mu_r w_1 l_{ef}}{h_1} \\ \Lambda_3 = \frac{\mu_0 \mu(B_{mb1}) w_{mb1} l_{ef}}{l_{mb1}} \\ \Lambda_4 = \frac{\mu_0 (l_1 + l_2 + l_3) l_{ef}}{2l_{mb1}} \\ \Lambda_5 = \frac{\mu_0 \mu(B_{mb2}) w_{mb2} l_{ef}}{h_1} \end{cases} \tag{23}$$

F_{sd} is the stator d-axis armature MMF, R_{gd} is the air gap reluctance at half pole pitch, R_m and R_l are the PM reluctance and the magnetic barrier reluctance respectively. The d-axis armature magnetic field EMC model is shown in Fig. 7.

For the I-type rotor structure studied in this paper, when only the q-axis current source acts, the flux path does not pass through the PM, and the rotor bridge area is not saturated. To simplify the calculation, it is considered that the magnetic potential of the q-axis rotor is 0.

IV. TORQUE CALCULATION

A. MODULATION OF AIR-GAP RELATIVE PERMEANCE

According to the motor air gap magnetic field modulation theory [25], the air gap magnetic potential is modulated by the air gap relative permeance function generated by the stator open slot.

The stator MMF is calculated by (11) and can be expressed after modulation by the air gap relative permeance as:

$$F_{s\_s}(\theta, t) = F_s(\theta, t)\Lambda_s(\theta)$$

$$\int_{0+wt}^{\frac{\alpha_p}{2}\pi+wt} (F_{sd} - F_{rd}) \cdot \frac{\mu_0}{pg_e} r_g l_{ef} \mathrm{d}\theta = F_{rd} \left(\frac{\mu_0 \mu_r w_1 l_{ef}}{h_1} + \frac{\mu_0 \mu(B_{mb1}) w_{mb1} l_{ef}}{l_{mb1}} + \frac{\mu_0 (l_1 + l_2 + l_3) l_{ef}}{2h_1} + \frac{\mu_0 \mu(B_{mb2}) w_{mb2} l_{ef}}{h_1} \right) \tag{21}$$

$$F_{rd} = \frac{\Lambda_1 \sum_v \frac{2F_{sv}}{v} \cos(vwt - k_v wt + v\frac{\alpha_p \pi}{4}) \sin(v\frac{\alpha_p \pi}{4}) \cos(\varphi)}{\Lambda_1(\frac{\alpha_p \pi}{2}) + \Lambda_2 + \Lambda_3 + \Lambda_4 + \Lambda_5} \tag{22}$$

$$= \sum_{v} \Lambda_{s0} F_{sv} \cos(vp\theta - k_v wt + k_v\varphi) + \sum_{v}\sum_{k} \frac{\Lambda_{sk} F_{sv}}{2} \cos\left[(vp+kZ)\theta - k_v wt + k_v\varphi\right] + \sum_{v}\sum_{k} \frac{\Lambda_{sk} F_{sv}}{2} \cos\left[(vp-kZ)\theta - k_v wt + k_v\varphi\right] \tag{24}$$

As shown in (24), for the 36-slot, 8-pole PM motor, Z is an integer multiple of p, so the modulation only changes the amplitude of each harmonic, without affecting the speed and rotation direction. Fig. 8 shows the waveform and harmonic analysis comparison of stator armature MMF. After considering the modulation effect of the open slot, the magnetic permeance of the corresponding positions of the teeth and slots is different, so the stator MMF waveform is affected by the cogging effect. Then the tooth harmonic component increases and the fundamental component decreases.

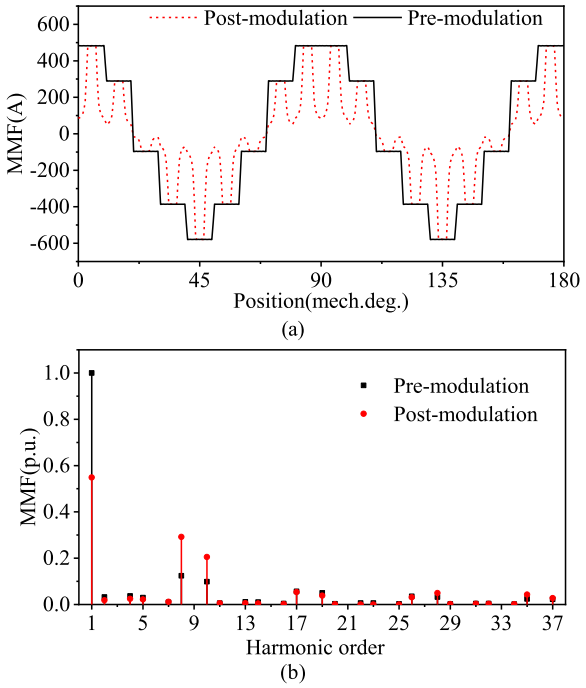

FIGURE 8. Stator MMF and harmonic analysis. (a) MMF. (b) Harmonic.

The RMP is modulated by the air gap relative permeance function and can be expressed as:

$$F_{r\_s}(\theta, t) = F_r(\theta, t)\Lambda_s(\theta) = \sum_{h=1,3,5\ldots}^{\infty} \Lambda_{s0} F_{rh} \cos(hp\theta - hwt) + \sum_{h=1,3,5\ldots}^{\infty}\sum_{k=1}^{\infty} \frac{\Lambda_{sk} F_{rh}}{2} \cos\left[(hp + kZ)\theta - hwt\right] + \sum_{h=1,3,5\ldots}^{\infty}\sum_{k=1}^{\infty} \frac{\Lambda_{sk} F_{rh}}{2} \cos\left[(hp - kZ)\theta - hwt\right] \tag{25}$$

As shown in (25), in addition to the odd harmonics contained in the original RMP, the $|hp \pm kZ|$th-order harmonic is introduced by modulation, and its speed is determined by the harmonic order h of the original RMP. The comparison of the waveform and harmonic analysis of the RMP is shown in Fig.9. It can be seen that even harmonics are introduced through modulation.

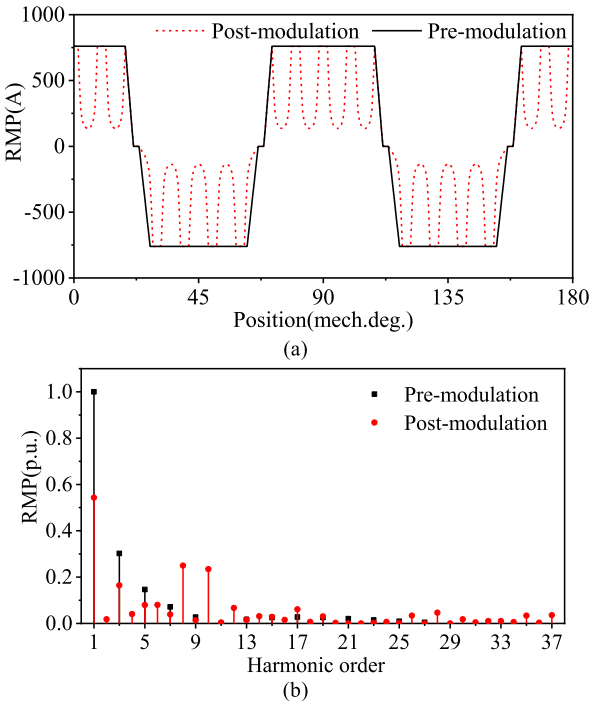

FIGURE 9. RMP and harmonic analysis. (a) RMP. (b) Harmonic.

To sum up, the original stator MMF contains $v \neq 3i$th-order harmonics. After the modulation function is applied, only the amplitude of each harmonic is changed, and the harmonic order remains unchanged. The original RMP contains $h = 2i + 1$th-order harmonics. After the modulation function is applied, the $|hp \pm kZ|$th-order harmonics are introduced. These harmonic times include $h = 2i$th-order, that is, the modulated RMP contains all harmonics.

B. TORQUE GENERATION MECHANISM

According to the modulated stator and rotor magnetic potential expressions, (7), (11), and (20) are substituted into (4), and the torque expression can be rewritten as:

$$T_e = -\frac{r_g l_{ef} \mu_0 p}{g} \int_0^{2\pi} \sum_{h=1}^{\infty} F_{rh} \cos(hp\theta - hwt) \cdot \left[\Lambda_{s0} + \sum_{h=1}^{\infty} \cos(kZ\theta)\right] \cdot \sum_{h=1}^{\infty} F_{sv} v \sin(vp\theta - k_v wt + k_v\varphi) \mathrm{d}\theta \tag{26}$$

When $vp = hp$ or $vp = |hp \pm kZ|$, (26) generates a torque that is not zero, then the motor instantaneous torque can be

expressed as:

$$T_e = pr_g l_{ef} \pi \frac{\mu_0}{2g} \sum_{v=1}^{\infty} \sum_{h=1}^{\infty} \sum_{k=1}^{\infty} vF_{sv} F_{rh} \Delta T_e$$

$$\Delta T_e = \begin{cases} 2\Lambda_{s0} \sin(hwt + k_v\varphi - k_v wt), vp = hp \\ \Lambda_{sk} \sin(hwt + k_v\varphi - k_v wt), hp + kZ = vp \\ \Lambda_{sk} \sin(\mathrm{sgn}(hp - kZ)hwt + k_v\varphi - k_v wt), \\ \qquad |hp - kZ| = vp \end{cases} \tag{27}$$

where: sgn is the sign function.

According to (27), to generate a constant torque, when $vp = hp$ and $vp = hp + kZ, h = k_v$ shall be met; when $vp = |hp - kZ|$, $\mathrm{sgn}(hp - kZ)h = k_v$ shall be met. That is, the average torque is generated by the action of the fundamental rotor magnetic field and the vth-order stator magnetic field with the same speed, v and h meet the above three equations, then the expression of the average torque can be expressed as:

$$T_{avg} = pr_g l_{ef} \pi \frac{\mu_0}{2g} \sum_{v=1}^{\infty} \sum_{h=1}^{\infty} \sum_{k=1}^{\infty} vF_{sv} F_{rh} \Delta T_{avg}$$

$$\Delta T_{avg} = \begin{cases} 2\Lambda_{s0} \sin(\varphi), v = h = 1 \\ \Lambda_{sk} \sin(\varphi), hp + kZ = vp, h = 1 \\ \Lambda_{sk} \sin(-\varphi), |hp - kZ| = vp, h = 1 \end{cases} \tag{28}$$

Since the stator MMF contains only the $3i + 1$ and $3i + 2$ harmonics, that is, $v \neq 3i$. in order to satisfy conditions $vp = hp$ and $vp = |hp \pm kZ|$, h can only be taken as $6i \pm 1$, after derivation the torque ripple as follows:

$$T_{ripple} = pr_g l_{ef} \pi \frac{\mu_0}{2g} \sum_{v=1}^{\infty} \sum_{h=1}^{\infty} \sum_{k=1}^{\infty} vF_{sv} F_{rh} \Delta T_{ripple}$$

$$\Delta T_{ripple} = \begin{cases} 2\Lambda_{s0} \sin(6iwt \pm \varphi), vp = hp \\ \Lambda_{sk} \sin(6iwt \pm \varphi), hp + kZ = vp \\ \Lambda_{sk} \mathrm{sgn}(hp - kZ) \sin(6iwt \pm \varphi), |hp - kZ| = vp \end{cases} \tag{29}$$

According to the analytical expressions of average torque and torque ripple in (28) and (29), It can be seen that on the premise of meeting the corresponding harmonic orders of the armature and rotor magnetic potential, when the speed of the stator MMF and the RMP is equal, the average torque will be generated, otherwise, the torque fluctuation will be generated, and the order of motor torque ripple is $6i$th.

It can be seen from the analysis that the torque generation mechanism of the PM motor with formed windings: the harmonic interaction of the corresponding order after the stator and rotor magnetic potential is modulated by the air-gap relative permeance function. Taking the formed windings PM motor with 36 slots and 8-pole as an example, the contribution of harmonic order of stator and rotor magnetic potential to torque is analyzed. According to the generation conditions of non-zero torque, the average torque is generated when the fundamental RMP interacts with fundamental MMF, stator MMF of 10th, 19th, 28th orders, and stator MMF of 8th, 17th, 26th orders respectively. When the harmonic order of the RMP is $6i \pm 1$, take the 5th and 7th as an example. When the above three conditions are met, the torque ripple will be generated by acting with the corresponding stator harmonic magnetic field respectively, the harmonic combination of magnetic potential generating average torque and torque ripple is shown in Table 3 and Table 4.

TABLE 4. Combinations that generate torque ripple.

condition	Λ_{sk}	F_{sv}	F_{rh}
$vp = hp$	$k = 0$	$v = 5$	$h = 5$
		$v = 7$	$h = 7$
$vp = hp + kZ$	$k = 1$	$v = 14$	$h = 5$
	$k = 2$	$v = 23$	
	$k = 1$	$v = 16$	$h = 7$
	$k = 2$	$v = 25$	
$vp = \lvert hp - kZ \rvert$	$k = 1$	$v = 4$	$h = 5$
	$k = 2$	$v = 13$	
	$k = 1$	$v = 2$	$h = 7$
	$k = 2$	$v = 11$	

V. FEM VERIFICATION

A. NO-LOAD MAGNETIC FIELD

Fig. 10 shows the no-load air gap magnetic density under different calculation methods. As shown in Fig. 10 (a), the two calculation methods agree well in amplitude and trend. Fig.10 (b) shows the harmonic analysis comparison under the two methods. The amplitude of the fundamental component obtained by FEM is 0.818T, and that of AM is 0.808T. Moreover, the amplitude of higher harmonics is also close. In addition to the odd harmonics such as the 3rd and 5th harmonics, Since the motor uses an open slot, it introduces a higher component of tooth harmonic, that is, the $v = k(Z/p) \pm 1, k = 1, 2, 3, \ldots$.th-order harmonic.

The no-load back electromotive force (EMF) is solved based on obtaining the no-load air gap magnetic density. The magnetic linkage generated by the single-turn coil is:

$$\psi_c = l_{ef} r_g \int_{-\frac{a_y}{2}}^{\frac{a_y}{2}} B_g(\theta, t) \mathrm{d}\theta \tag{30}$$

where: a_y is the coil pitch angle.

The no-load back EMF induced in single-phase winding can be expressed as:

$$E_\phi = -N \frac{\mathrm{d}\psi_c}{\mathrm{d}t} \tag{31}$$

Fig.11 shows the comparison of the no-load back-EMF. In Fig. 11 (a), the waveforms and trends obtained by the two methods are in good agreement. The amplitude of the main harmonic obtained by FEM and AM are 192.8V and 196.6V respectively, and the amplitude of the higher harmonic components are also relatively similar.

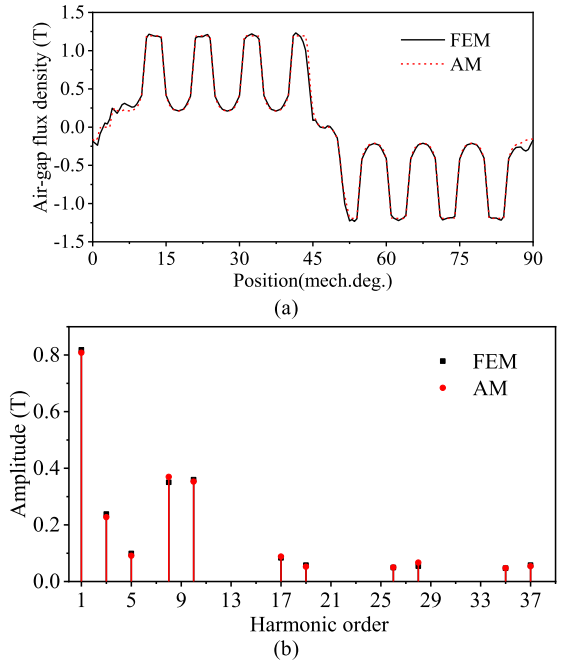

FIGURE 10. No-load air gap flux density. (a) Flux density. (b) Harmonic.

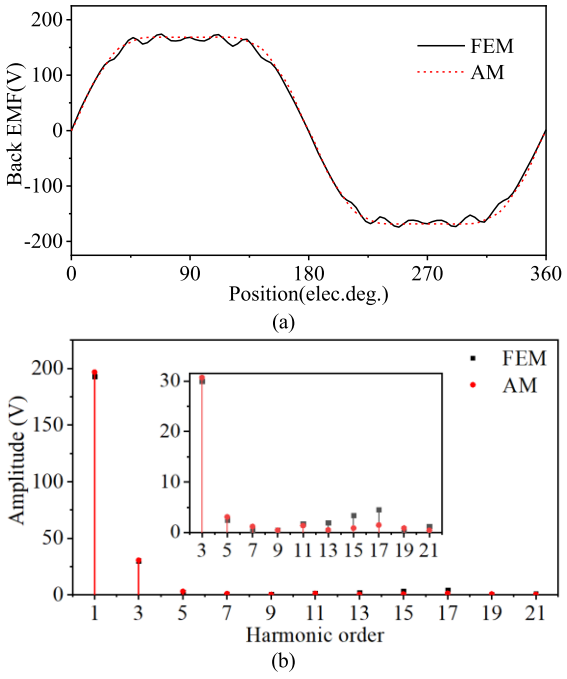

FIGURE 11. No-load back EMF. (a) Back EMF. (b) Harmonic.

B. ARMATURE REACTION MAGNETIC FIELD

According to the above analysis, the stator MMF and RMP generated by the stator current source are obtained. Considering the influence of stator slotting, the armature reaction flux density under different current angles is calculated. Fig.12 shows the comparison of armature reaction flux density at different current angles. Under the three conditions of d-axis ($\varphi = 0°$), q-axis ($\varphi = 90°$), and rated load ($\varphi = 45°$), the

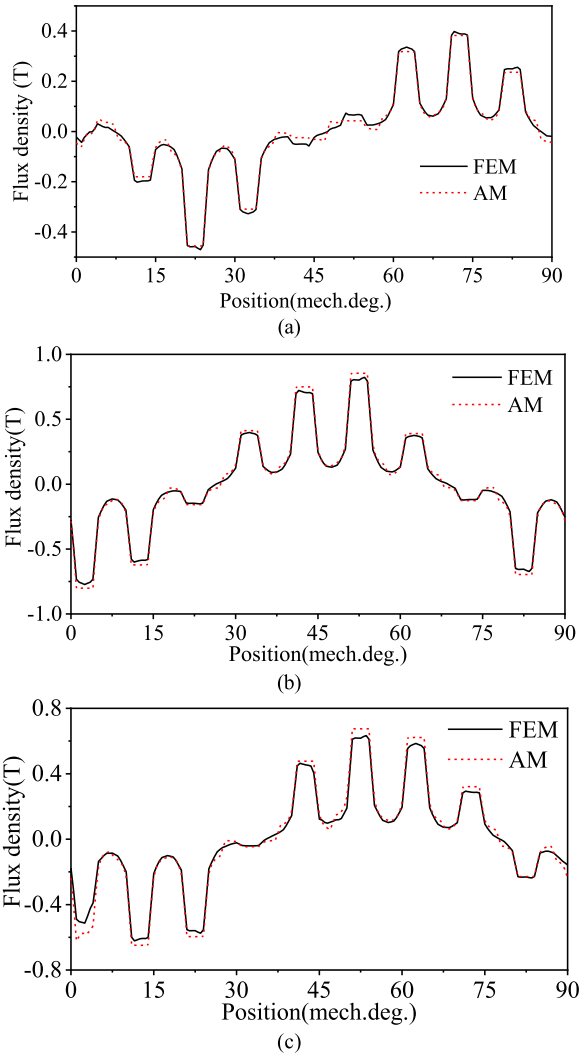

FIGURE 12. Armature reaction flux density. (a) D-axis ($\varphi = 0°$). (b) Q-axis ($\varphi = 90°$). (c) Rated working conditions ($\varphi = 45°$).

results calculated by AM and FEM are in good agreement, which verifies the correctness of the stator MMF and RMP obtained by the AM.

C. TORQUE

Under rated load conditions (current amplitude is 64.35A, the current angle is 45°, and speed of 2550rpm), the PM torque and reluctance torque waveforms of the motor obtained by FEM and AM are compared. Fig.13 shows the PM torque waveform of the traditional analytical method (am), the calculation method proposed in this paper (AM), and the finite element method (FEM), the average torque of the three is 49.125 Nm, 52.77 Nm, and 51.033 Nm respectively. Compared with the traditional analytical method, the calculation result of the analytical method proposed in this paper is closer to the finite element method. Set the material of the PM to air to obtain the reluctance torque waveform as shown in Fig. 14. In the FEM, the reluctance torque accounts for 10.08% of

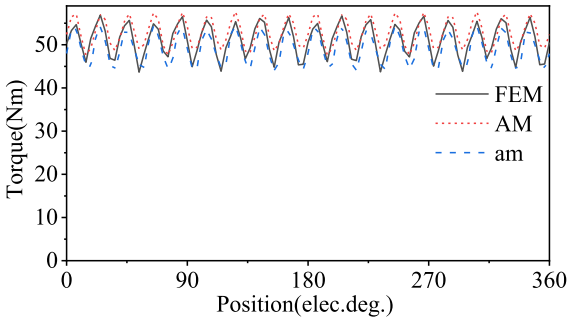

FIGURE 13. Comparison of PM torque.

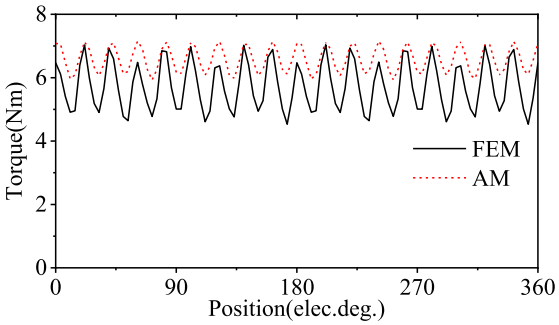

FIGURE 14. Comparison of reluctance torque.

the total torque, and in the AM, the proportion is 11.02%. There is an error between the AM and the FEM in solving the waveform, which is due to the failure of the AM to consider the effect of PMs on the reluctance torque.

For IPM motors, the electromagnetic torque is equal to the superposition of the PM torque and the reluctance torque. Fig. 15 shows the waveforms comparison of electromagnetic torque waveform under rated load conditions (current amplitude of 64.35A, current angle of 45°, and speed of 2550rpm). According to Fig.15 (a), the average electromagnetic torque in the FEM is 56.76Nm, the PTP torque is 14.586Nm and the torque ripple is 25.7%; in the AM, the three are 59.239Nm, 13.363Nm, and 22.557% respectively. Although there is some error in constant torque, the PTP torque and torque fluctuation are similar for both methods, indicating that the waveforms and trends of the two calculations are in good agreement. Harmonic analysis of the electromagnetic torque waveforms under the two methods yielded a comparison graph as shown in Fig.15(b). The fundamental component of the electromagnetic torque for the FEM and the AM are 56.76Nm and 59.239Nm respectively, the harmonic components mainly consist of the 6th, 12th, and 18th order, and the 6th, 12th, and 18th harmonics obtained by FEM are 1.176Nm, 0.773Nm and 5.263Nm, while the AM is 0.334Nm, 0.49Nm and 4.526 Nm. Among them, the 18th harmonic component is large, because according to (29), under the premise of satisfying conditions $vp = hp$ and $vp = |hp \pm kZ|$, the stator and rotor magnetic potentials interact, and the corresponding $vF_{sv}F_{rh}$ is greater when the

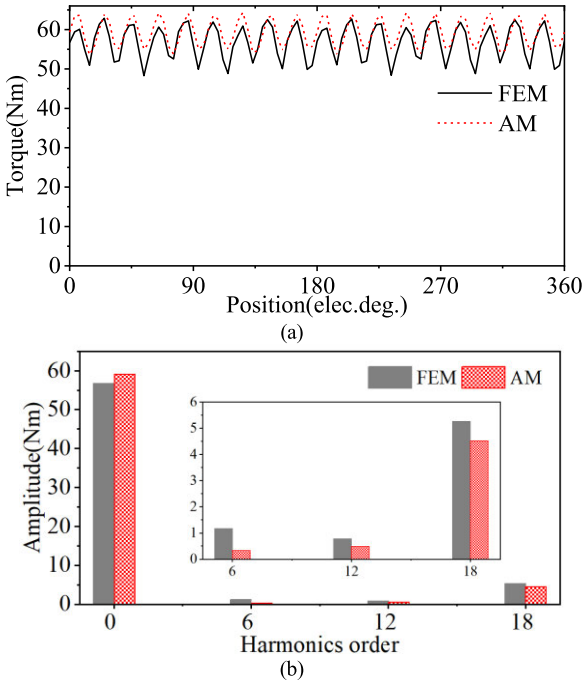

FIGURE 15. Comparison of Electromagnetic Torque. (a) Electromagnetic Torque. (b) Harmonic.

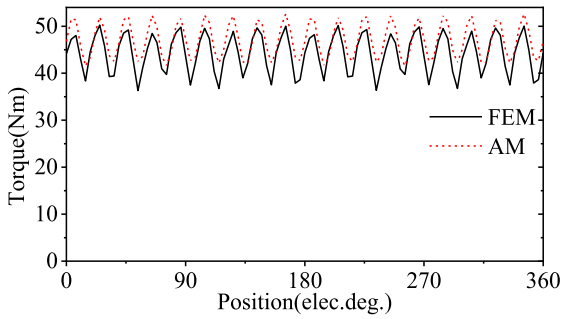

FIGURE 16. Comparison of electromagnetic torque at 0.8 times rated load.

18th harmonic is generated. There is a certain difference in the harmonic amplitude of the two methods, which is caused by the approximate equivalent model used in the AM. The order of harmonics is also consistent with the theoretical derivation of the 6*i*th-order.

Fig. 16 shows the comparison diagram of electromagnetic torque waveform under 0.8 times rated load (current amplitude of 51.48A, current angle of 45°, and speed of 2550rpm). In the calculation results of FEM, the average value of electromagnetic torque is 44.395Nm, the PTP value is 13.927Nm, and the torque fluctuation is 31.37%; In the AM, the three are 47.023Nm, 12.078Nm and 25.69% respectively. The waveform and trend of the two calculation results are highly consistent, which verifies the correctness of the AM to calculate the motor torque.

Fig.17 shows the various characteristics of different torque components of the motor with the current angle under the

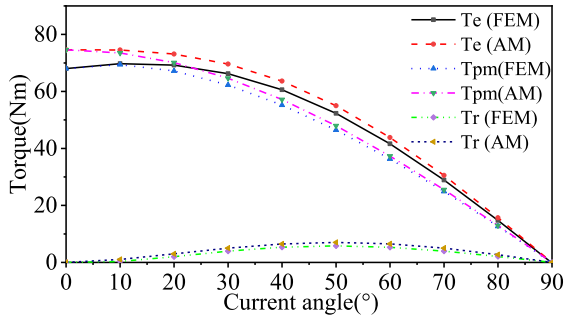

FIGURE 17. Torque-current angle characteristics.

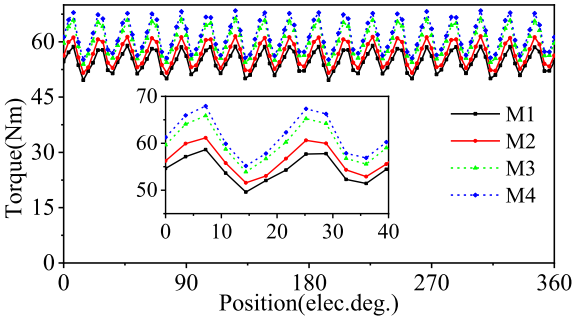

FIGURE 18. Torque-slot opening width characteristics.

rated current of 64.35A. It can be seen that the PM torque (T_{pm}), reluctance torque (T_r), and electromagnetic torque (T_e) are in good consistency in the FEM and AM within the current angle range of 0° to 90°.

Fig. 18 shows the various characteristics of torque with slot opening width under rated load conditions, and the average torque and torque ripple under different slot opening widths are calculated according to the proposed torque analysis model. The corresponding slot opening widths of M1, M2, M3, and M4 are 8.5mm, 9mm, 9.5mm, and 10mm respectively. As shown in the enlarged figure in Fig.18, the torque ripples increase sequentially as the slot opening width increases, and the corresponding torque ripples of M1, M2, M3, and M4 are 9.066Nm, 9.6Nm, 11.98Nm, and 12.758Nm respectively. Therefore, the proposed torque calculation model can reflect the influence of electromagnetic parameters such as slot opening width on the torque characteristics.

VI. CONCLUSION

In this paper, firstly the magnetic field of permanent magnet motors with formed windings is calculated based on the magnetic potential-permeance theory. By analyzing the modulation effect of the stator slotting on the stator MMF and RMP, the torque analytical model is established based on the modulation function, stator MMF and RMP, then the torque generation mechanism is analyzed and the different torque components are solved. The conclusions are as follows:

1) The armature reaction magnetic field and rotor PM magnetic field based on winding function and EMC method are consistent with the FEM, which verifies the correctness of the RMP generated by the PM, the MMF, and the RMP generated by the stator armature current.
2) The modulation function of stator slotting, which only changes the amplitude of each harmonic of stator MMF, and does not affect the speed and rotation direction; It brings the $|hp \pm kZ|$th-order harmonic in the RMP, and its speed is determined by the harmonic order h of the original RMP.
3) The torque analysis model based on the modulation function, stator MMF and RMP can obtain the generation mechanism of average torque and torque ripple, which reflects the law of interaction between stator MMF and RMP on torque characteristics under the modulation of stator relative permeance when the corresponding harmonic order relationship is satisfied, and the order of torque ripple is $6i$.
4) Under the rated load condition, the average electromagnetic torque is 56.76Nm, the PTP torque is 14.586Nm, and the torque ripple is 25.7% in the finite element simulation results. In the derived torque analysis model, the three are 59.239Nm, 13.363Nm, and 22.557%, respectively. The waveform and trend of the two calculation results have a high degree of agreement, which verifies the accuracy of the torque analysis model.

REFERENCES

[1] M. Popescu, J. Goss, D. A. Staton, D. Hawkins, Y. C. Chong, and A. Boglietti, "Electrical vehicles-practical solutions for power traction motor systems," *IEEE Trans. Ind. Appl.*, vol. 54, no. 3, pp. 2751–2762, May 2018.

[2] M. Polat, A. Yildiz, and R. Akinci, "Performance analysis and reduction of torque ripple of axial flux permanent magnet synchronous motor manufactured for electric vehicles," *IEEE Trans. Magn.*, vol. 57, no. 7, pp. 1–9, Jul. 2021.

[3] M. S. Islam, I. Husain, A. Ahmed, and A. Sathyan, "Asymmetric bar winding for high-speed traction electric machines," *IEEE Trans. Transport. Electrific.*, vol. 6, no. 1, pp. 3–15, Mar. 2020.

[4] E. Preci, S. Nuzzo, G. Valente, D. Gerada, D. Barater, M. Degano, G. Buticchi, and C. Gerada, "Segmented hairpin topology for reduced losses at high-frequency operations," *IEEE Trans. Transport. Electrific.*, vol. 8, no. 1, pp. 688–698, Mar. 2022.

[5] Y. Zhao, D. Li, T. Pei, and R. Qu, "Overview of the rectangular wire windings AC electrical machine," *CES Trans. Electr. Mach. Syst.*, vol. 3, no. 2, pp. 160–169, Jun. 2019.

[6] H.-C. Liu, H.-J. Lee, H.-S. Seol, S. Cho, J. Lee, and Y. J. Oh, "Optimal slot design of IPMSM in railway with independently rotating wheelsets," *IEEE Trans. Magn.*, vol. 55, no. 2, pp. 1–4, Feb. 2019.

[7] W. Cheng, G. Cao, Z. Deng, L. Xiao, and M. Li, "Torque comparison between slotless and slotted ultra-high-speed AFPM motors using analytical method," *IEEE Trans. Magn.*, vol. 58, no. 2, pp. 1–5, Feb. 2022.

[8] G. Liu, Y. Wang, Q. Chen, G. Xu, and D. Cao, "Design and analysis of a new equivalent magnetic network model for IPM machines," *IEEE Trans. Magn.*, vol. 56, no. 6, pp. 1–12, Jun. 2020.

[9] B. Guo, Y. Huang, F. Peng, and J. Dong, "General analytical modeling for magnet demagnetization in surface mounted permanent magnet machines," *IEEE Trans. Ind. Electron.*, vol. 66, no. 8, pp. 5830–5838, Aug. 2019.

[10] Y. Zhu, G. Liu, L. Xu, W. Zhao, and D. Cao, "A hybrid analytical model for permanent magnet Vernier machines considering saturation effect," *IEEE Trans. Ind. Electron.*, vol. 69, no. 2, pp. 1211–1223, Feb. 2022.

[11] H. Chen, D. Li, R. Qu, Z. Zhu, and J. Li, "An improved analytical model for inductance calculation of interior permanent magnet machines," *IEEE Trans. Magn.*, vol. 50, no. 6, pp. 1–8, Jun. 2014.
[12] G. Liu, L. Liu, Q. Chen, and W. Zhao, "Torque calculation of five-phase interior permanent magnet machine using improved analytical method," *IEEE Trans. Energy Convers.*, vol. 34, no. 2, pp. 1023–1032, Jun. 2019.
[13] P. Liang, Y. Pei, F. Chai, Y. Bi, and S. Cheng, "An improved method for armature-reaction magnetic field calculation of interior permanent magnet motors," *IEEE Trans. Magn.*, vol. 52, no. 7, pp. 1–4, Jul. 2016.
[14] Z. Q. Zhu, B. Lee, L. Huang, and W. Chu, "Contribution of current harmonics to average torque and torque ripple in switched reluctance machines," *IEEE Trans. Magn.*, vol. 53, no. 3, pp. 1–9, Mar. 2017.
[15] D. Spalek, "Generalization of Maxwell stress tensor method for magnetically anisotropic regions," *IEEE Trans. Magn.*, vol. 55, no. 12, pp. 1–6, Dec. 2019.
[16] Y. Lu, J. Li, R. Qu, D. Ye, H. Lu, J. Sun, M. Ge, and H. Xu, "Electromagnetic force and vibration analysis of permanent-magnet-assisted synchronous reluctance machines," *IEEE Trans. Ind. Appl.*, vol. 54, no. 5, pp. 4246–4256, Oct. 2018.
[17] N. Bianchi, S. Bolognani, D. Bon, and M. D. Pré, "Torque harmonic compensation in a synchronous reluctance motor," *IEEE Trans. Energy Convers.*, vol. 23, no. 2, pp. 466–473, Jun. 2008.
[18] R. Zhou, G. Li, Q. Wang, and J. He, "Torque calculation of permanent-magnet spherical motor based on permanent-magnet surface current and Lorentz force," *IEEE Trans. Magn.*, vol. 56, no. 5, pp. 1–9, May 2020.
[19] W. Su, Y. Guo, D. Wang, and K. Wei, "Semi-analytical calculation of no-load radial and tangential electromagnetic force waves of a non-salient pole synchronous generator," *IEEE Trans. Energy Convers.*, vol. 36, no. 4, pp. 2956–2966, Dec. 2021.
[20] L. Wu, H. Yin, D. Wang, and Y. Fang, "A nonlinear subdomain and magnetic circuit hybrid model for open-circuit field prediction in surface-mounted PM machines," *IEEE Trans. Energy Convers.*, vol. 34, no. 3, pp. 1485–1495, Sep. 2019.
[21] L. R. Huang, J. H. Feng, S. Y. Guo, J. X. Shi, W. Q. Chu, and Z. Q. Zhu, "Analysis of torque production in variable flux reluctance machines," *IEEE Trans. Energy Convers.*, vol. 32, no. 4, pp. 1297–1308, Dec. 2017.
[22] Q. Chen, G. Xu, G. Liu, W. Zhao, Z. Lin, and L. Liu, "Torque ripple reduction in five-phase IPM motors by lowering interactional MMF," *IEEE Trans. Ind. Electron.*, vol. 65, no. 11, pp. 8520–8531, Nov. 2018.
[23] H. Mahmoud, N. Bianchi, G. Bacco, and N. Chiodetto, "Nonlinear analytical computation of the magnetic field in reluctance synchronous machines," *IEEE Trans. Ind. Appl.*, vol. 53, no. 6, pp. 5373–5382, Nov./Dec. 2017.
[24] P. Liang, Y. Pei, F. Chai, and K. Zhao, "Analytical calculation of *D*- and *Q*-axis inductance for interior permanent magnet motors based on winding function theory," *Energies*, vol. 9, no. 8, p. 580, Jul. 2016.
[25] M. Cheng, P. Han, and W. Hua, "General airgap field modulation theory for electrical machines," *IEEE Trans. Ind. Electron.*, vol. 64, no. 8, pp. 6063–6074, Aug. 2017.

KE ZHANG was born in Nanyang, China, in 1995. He received the B.Sc. degree from the Harbin University of Science and Technology, in 2018, where he is currently pursuing the Ph.D. degree. His current research interests include permanent magnet synchronous motor design and electromagnetic calculation.

YANPING LIANG was born in Harbin, China, in 1963. She received the M.S. degree in electrical machines from the Harbin University of Science and Technology, Harbin, in 1988, and the Ph.D. degree in electrical machines from the Harbin Institute of Technology, Harbin, in 2005. She is currently a Professor with the Harbin University of Science and Technology. Her research interests include electromechanical energy conversion mechanism and calculation of electromagnetic devices, electromagnetic theory, and electromagnetic design of motors.

XU BIAN was born in Harbin, China, in 1988. She received the B.Sc., M.Sc., and Ph.D. degrees from the Harbin University of Science and Technology, in 2010, 2013, and 2016, respectively. She was with the Harbin University of Science and Technology, where she is currently a Professor with the School of Electrical and Electronic Engineering. Her research interests include basic theory, operation analysis, and design method of special and new motors.

PEIPEI YANG was born in Hebei, China, in 1993. She is currently pursuing the Ph.D. degree in electrical machines with the Harbin University of Science and Technology, Harbin, China. Her research interest includes electromagnetic and thermal analysis of electrical machines.